ACS APPLIED MATERIALS & INTERFACES

www.acsami.org

Research Article

Dual-Functional Electrolyte Additives toward Long-Cycling Lithium-Ion Batteries: Ecofriendly Designed Carbonate Derivatives

Jung-Gu Han,[#] Eunbyul Hwang,[#] Yoseph Kim,[#] Sewon Park, Koeun Kim, Deok-Ho Roh, Minsu Gu, Sang-Ho Lee, Tae-Hyuk Kwon, Youngjo Kim,* Nam-Soon Choi,* and Byeong-Su Kim*

Cite This: *ACS Appl. Mater. Interfaces* 2020, 12, 24479−24487

Read Online

ACCESS | Metrics & More | Article Recommendations | Supporting Information

ABSTRACT: Long-term stability of the solid electrolyte interphase (SEI) and cathode−electrolyte interface (CEI) layers formed on anodes and cathodes is imperative to mitigate the interfacial degradation of electrodes and enhance the cycle life of lithium-ion batteries (LIBs). However, the SEI on the anode and CEI on the cathode are vulnerable to the reactive species of PF_5 and HF produced by the decomposition and hydrolysis of the conventional $LiPF_6$ electrolyte in a battery inevitably containing a trace amount of water. Here, we report a new class of cyclic carbonate-based electrolyte additives to preserve the integrity of SEI and CEI in LIBs. This new class of additives is designed and synthesized by an ecofriendly approach that involves fixing CO_2 with functional epoxides bearing various reactive side chains. It was found that the cyclic carbonates of 3-(1-ethoxyethoxy)-1,2-propylene carbonate and 3-trimethoxysilylpropyloxy-1,2-propylene carbonate, possessing high capability for the stabilization of Lewis-acidic PF_5, exhibit a capacity retention of 79.0% after 1000 cycles, which is superior to that of the pristine electrolyte of 54.7%. Moreover, TMSPC has HF-scavenging capability, which, along with PF_5 stabilization, results in enhanced rate capability of commercial $LiNi_{0.6}Mn_{0.2}Co_{0.2}O_2$ (NCM622)/graphite full cells, posing a significant potential for high-energy-density LIBs with long cycle stability.

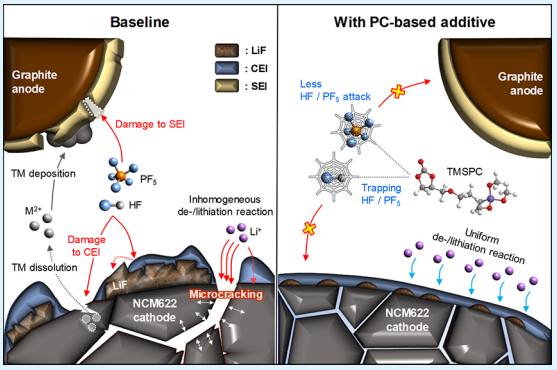

KEYWORDS: *lithium-ion batteries, electrolyte additives, PF_5 stabilization, HF scavenging, $LiPF_6$-based electrolytes*

INTRODUCTION

With increasing environmental and energy issues such as global warming, as well as the environmental pollution caused by the depletion of fossil fuels, lithium-ion batteries (LIBs) have emerged as among the most environmentally friendly technologies that can significantly reduce the dependence on fossil fuels and mitigate CO_2 emission.[1,2] In addition, there has been a recent surge of interests in grid/utility-energy storage systems and electric vehicles. This has driven the development of large-scale LIBs with high energy density compared to that of the conventional LIBs used in small electronic devices.[3−6] To surmount the high-end requirements for energy storage systems and electric vehicles, it continues to be a challenging endeavor to develop high-capacity electrode materials for LIBs as well as the other key components including separators and electrolyte materials.[7,8] Although lithium hexafluorophosphate ($LiPF_6$)-based electrolytes have been widely used in commercialized LIBs owing to their high ionic conductivity and excellent electrochemical stability, their poor stability toward moisture and heat often poses significant issues.[9−11] In particular, residual moisture on the cathode surface can facilitate the hydrolysis of $LiPF_6$ salts, resulting in the generation of highly reactive acidic species such as POF_3, PF_5, and HF. This can be detrimental to the operation of LIBs due to (1) irrevocable damage of the solid electrolyte interphase (SEI) and cathode−electrolyte interface (CEI) layer on the electrodes,[12] (2) triggering of transition-metal dissolution,[13] and (3) the decomposition of electrolyte solvent molecules.[14] Therefore, it is vital to scavenge the acid compounds produced by $LiPF_6$. Thus far, this prevailing concern was addressed using a functional electrolyte additive such as a HF/PF_5 scavenger to improve the electrochemical performance of LIBs. For example, dimethoxydimethylsilane (DODSi) is a well-known HF scavenger.[15] The H^+ generated from HF interacts with the O atom in DODSi, while the Si in DODSi affords a Si−F bond with F^- in HF, resulting in the formation of $SiF_2(CH_3)_2$. An aminosilane-containing HF scavenger has also been reported with heptamethyldisilazane (HMDS).[16−18] After storage for a week at room temperature,

Received: March 7, 2020
Accepted: May 5, 2020
Published: May 5, 2020

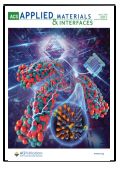

the HF content in the electrolytes remarkably decreased from 266.8 to 50.5 ppm only with 0.1 wt % HMDS-containing electrolyte.[16] Along the same lines, our group recently reported that tris(trimethylsilyl)phosphite (TMSPi) can serve as the most effective HF scavenger among trivalent phosphorous-(III)-based electrolyte additives.[19−22] In addition to the phosphite group, the three silyl ether groups can strongly bind with F^- to produce trimethylsilyl fluoride through the formation of a pentavalent silane intermediate.[20] Unlike these examples, herein, we introduce a new class of electrolyte additives based on a cyclic carbonate derivative, which would eliminate issues related to the solubility and compatibility of additives with $LiPF_6$-based electrolyte systems.

Here, we present that the cyclic carbonates are synthesized by the insertion of CO_2 in functional epoxides bearing various reactive side chains. This ecofriendly method provides a new route to utilizing CO_2 for functional electrolyte additives in LIBs. Moreover, these electrolyte additives are designed to stabilize PF_5 by the incorporation of oxygen as a Lewis base with a high affinity toward the Lewis-acidic PF_5; this mitigates HF generation. In addition, one of the designed electrolyte additives has silyl ether (Si−O) moieties, which afford the formation of strong Si−F intermediates with the F^- of HF, resulting in HF scavenging. These new electrolyte additives are expected to address several key issues caused by the highly reactive species of HF and PF_5 in $LiPF_6$-based electrolytes. Furthermore, the effective role of the functional electrolyte additives is carefully elucidated by investigating their scavenging ability toward the fatal reactive species generated from $LiPF_6$ in the electrolyte and the surface chemistry of high Ni cathodes and graphite anodes. We anticipate that this study opens a new avenue to achieve advanced applications of high-energy-density LIBs.

EXPERIMENTAL SECTION

Chemicals. Glycidol (Sigma-Aldrich; 96%), ethyl vinyl ether (Sigma-Aldrich; 99%, with 0.1% KOH as a stabilizer), and methyl iodide (Daejung Chemicals; 99%) were stored at 0 °C before use. 2,3-Dihydrofuran (Thermo Fisher Scientific; >98%), 3,4-dihydro-2*H*-pyran (Sigma-Aldrich; 97%), *p*-toluenesulfonic acid monohydrate (*p*-TsOH, Sigma-Aldrich; >98%), dichloromethane (DCM, Daejung Chemicals; 99.5%), sodium hydrogen carbonate (Daejung Chemicals; >99%), 4-*tert*-butylphenol (Sigma-Aldrich; >98%), *N*,*N*-dimethylethylenediamine (Sigma-Aldrich; >98%), formaldehyde (Alfa Aesar; 37% in aqueous solution, ACS, 36.8−38.0%, stabilized with 10−15% methanol), and carbon dioxide (Special Gas, Inc.; >99.999%) were used as received. The NMR solvent, $CDCl_3$, was purchased from Cambridge Isotope Laboratories, and tetrahydrofuran (THF)-d_8 was purchased from BK Instruments Inc.

Synthesis of Epoxide Compounds. 1-Ethoxyethyl glycidyl ether (EEGE), tetrahydrofuranyl glycidyl ether (TFGE), and tetrahydropyranyl glycidyl ether (TPGE) were synthesized according to the literature.[23−25]

Representative Procedures for the Insertion Reaction of CO_2 in Epoxide Compounds. All manipulations were performed under an atmosphere of dinitrogen using standard Schlenk glassware with a dual manifold Schlenk line.[26,27] Dinitrogen was deoxygenated using an activated Cu catalyst and then dried with drierite.[28] Carbon dioxide (99.999%) was used as received without further purification. Diethyl ether was purified by a Grubbs solvent purification system under a nitrogen atmosphere and stored over activated molecular sieves (4 Å).[29] An organocatalyst, 2-(bis(5-(*tert*-butyl)-2-hydroxybenzyl)amino)-*N*,*N*,*N*-trimethylethan-1-aminium iodide, was prepared according to the literature.[30] Functional epoxides (10 mmol) and the organocatalyst (110 mg, 0.20 mmol) were charged into a 15 mL stainless steel autoclave. The autoclave was pressurized to 10 bar of CO_2 and the reaction mixture was stirred at 80 °C for 12 h, after which the reactor was cooled and vented. All volatiles were removed in vacuo, and the precipitated catalyst was removed by filtration. The conversion of epoxide into the corresponding cyclic carbonate was verified by ^{1}H NMR spectroscopy. The cyclic carbonates were purified by column chromatography, and their structures were analyzed by various techniques such as NMR spectroscopy and mass spectrometry (Figures S1−S5).

3-(1-Ethoxyethoxy)-1,2-propylene Carbonate (EEPC). ^{1}H NMR ($CDCl_3$): δ 4.80 (m, 1H), 4.72 (m, 1H), 4.45 (m, 1H), 4.32 (m, 1H), 3.43−3.80 (m, 2H), 1.28 (dd, J_1 = 1.75 Hz, J_2 = 4.95 Hz, 3H), 1.17 (m, 3H). ^{13}C NMR ($CDCl_3$): δ 154.9 (d), 99.55 (d), 74.75, 66.11 (d), 63.18 (d), 61.18 (d), 19.28 (d), 15.06 (d). HRMS *m*/*z* calcd for $[C_8H_{14}O_5 + Na]$ 213.0739. Found: 213.0733.

3-Tetrahydrofuranyloxy-1,2-propylene Carbonate (TFPC). ^{1}H NMR ($CDCl_3$): δ 5.09 (q, J_1 = 3.7 Hz, J_2 = 3.4 Hz, 1H), 4.79 (dd, J_1 = 3.15 Hz, J_2 = 2.6 Hz, 1H), 4.27−4.48 (m, 2H), 3.52−3.91 (m, 4H), 1.77−1.99 (m, 4H). ^{13}C NMR ($CDCl_3$): δ 154.9 (d), 104.1 (d), 74.88 (d), 67.34 (d), 66.27 (d), 66.00 (d), 32.29 (d), 23.15 (d). HRMS *m*/*z* calcd for $[C_8H_{12}O_5 + Na]$ 211.0582. Found: 211.0577.

3-Tetrahydropyranyloxy-1,2-propylene Carbonate (TPPC). ^{1}H NMR ($CDCl_3$): δ 4.80−4.87 (m, 1H), 4.60−4.65 (m, 1H), 4.34−4.51 (m, 2H), 3.48−3.98 (m, 4H), 1.48−1.80 (m, 6H). ^{13}C NMR ($CDCl_3$): δ 154.9 (d), 98.65 (d), 74.94 (d), 66.31 (d), 66.23 (d), 61.93 (d), 30.13 (d), 25.16 (d), 18.74 (d). HRMS *m*/*z* calcd for $[C_9H_{14}O_5 + Na]$ 225.0739. Found: 225.0733.

3-Trimethoxysilylpropyloxy-1,2-propylene Carbonate (TMSPC). ^{1}H NMR ($CDCl_3$): δ 4.78 (m, 1H), 4.46 (m, 1H), 4.36 (m, 1H), 3.64 (m, 2H), 3.45 (s, 9H), 3.44 (m, 2H), 1.64 (m, 2H), 0.58 (m, 2H). ^{13}C NMR ($CDCl_3$): δ 154.8, 74.99, 73.44, 69.28, 65.95, 50.12, 22.34, 4.70. HRMS *m*/*z* calcd for $[C_{10}H_{20}O_7 + Na]$ 303.0876. Found: 303.0871.

Computational Details. Density functional theory (DFT)[31] calculations were performed with the Gaussian09 package.[32] The optimized ground-state geometries, as well as the highest occupied molecular orbital (HOMO) and lowest unoccupied molecular orbital (LUMO) energy levels of the carbonate additives, were obtained in the vacuum state using the hybrid functional B3LYP and the 6-311G +(3df,2p) basis set.

Electrolytes and Electrodes. The cyclic carbonate-based electrolyte additives (0.5 wt %) were incorporated into 1 M lithium hexafluorophosphate ($LiPF_6$) dissolved in a solvent mixture of ethylene carbonate (EC) and ethylmethyl carbonate (EMC) in a volume ratio of 3:7. The oxidation and reduction tendencies of the various carbonate-based electrolytes and additives were predicted by calculating the HOMO with DFT. To evaluate the effect of the functional additives on the electrochemical performance, the cathode was prepared by spreading a slurry mixture of 92.5 wt % $LiNi_{0.6}Mn_{0.2}Co_{0.2}O_2$ (NCM622, L&F Co., Ltd., secondary particles, ∼5−6 μm) as an active material, 3 wt % carbon black and 1.5 wt % SFG6 as conducting materials, and 3 wt % poly(vinylidene fluoride) (PVDF) binder dissolved in anhydrous *N*-methyl-2-pyrrolidinone (NMP, 99.5%, Sigma-Aldrich). The anode was prepared by spreading a slurry mixture of 96.6 wt % artificial graphite (S360, Fujian, ∼18−20 μm) as an active material, 1 wt % SFG6 (Timcal) as a conducting material, and 2.4 wt % binder (1.4 wt % styrene−butadiene rubber (SBR, BM-154B, Zeon) and 1 wt % carboxyl methylcellulose (CMC, MAC-350H, Sunrose)) dissolved in distilled water.

The mass loadings of the cathode and anode were 18 and 9.3 mg cm^{-2}, respectively. The areal capacity ratio of the negative and positive electrodes (N/P ratio) of the NCM622/graphite full cell was 1.05. The areal capacity of the NCM622/graphite full cell was 3.0 mAh cm^{-2}. A polyethylene membrane (PE, SK Innovation Co., Ltd.) was employed as a separator; its thickness and porosity were 20 μm and 38%, respectively.

Electrochemical Measurements. Electrochemical tests were performed using 2032 coin-type NCM622/graphite full cells assembled in an argon-filled glovebox. NCM622/graphite full cells were galvanostatically precycled at a rate of C/10 between 3.0 and 4.2 V using a computer-controlled battery measurement system

https://dx.doi.org/10.1021/acsami.0c04372
ACS Appl. Mater. Interfaces 2020, 12, 24479−24487

(WonATech WBCS 3000). Thereafter, the cells were cycled at a current density of 3.0 mA cm^{-2} (corresponding to 1C rate) in the potential window from 3.0 to 4.2 V for 1000 cycles at 25 °C. The rate capability of the full cells was evaluated at a fixed charge C rate (C/2) and various discharge C rates (C/2, 1C, 2C, and 3C).

Characterizations. To confirm the successful synthesis of the functional cyclic carbonates, ^{1}H NMR (400 MHz) spectra were acquired using an Avance III HD NMR spectrometer (Bruker). All spectra were recorded in ppm units with the deuterated solvent $CDCl_3$. To examine the surface chemistry and morphological changes of the electrodes, the cycled cells were carefully disassembled in a glovebox. The electrodes were rinsed in dimethyl carbonate (DMC) to remove the residual $LiPF_6$-based electrolyte and dried at room temperature. The components of the electrode−electrolyte interface on the NCM622 cathode and graphite anode were identified by ex situ X-ray photoelectron spectroscopy (XPS, Scientific K-Alpha system, Thermo Scientific) with Al Kα radiation under ultrahigh vacuum. All XPS spectra were calibrated by the hydrocarbon peak at a binding energy of 284.8 eV. All samples were prepared in a glovebox and sealed with an Al pouch film under vacuum before use. The morphology and structure of the NCM622 cathodes and graphite anodes were studied by field-emission scanning electron microscopy (FE-SEM, JSM-6700F, JEOL) in a high-vacuum environment. To analyze the surface components of the CEI on the electrode surface, time-of-flight secondary ion mass spectrometry (TOF-SIMS, ION-TOF GmbH, TOF-SIMS 5) was performed in ultrahigh vacuum at a pressure below 1.1 × 10^{-9} mbar. A pulsed 25 keV Bi1+ (1 pA) ion beam set in either the high-current mode or the burst alignment mode was applied for surface spectroscopy or image mapping. The typical analyzed area was 100 μm × 100 μm. ^{19}F NMR (377 MHz, Avance III HD NMR spectrometer, Bruker) spectra were acquired in the THF-d_8 solvent. The cyclic carbonate-based electrolyte additives (0.5 wt %) were added into 1.0 M $LiPF_6$ dissolved in a solvent mixture of EC and EMC in a volume ratio of 3:7. The samples for ^{19}F NMR analysis were prepared by the addition of 300 ppm of DI water to electrolytes with or without additives. Then, the electrolyte solutions were stored at 25 °C for 24 h. ^{19}F NMR spectra for the stored electrolytes were acquired in the THF-d_8 solvent.

RESULTS AND DISCUSSION

Synthesis of Carbonate-Based Additives from the Coupling Reaction of Epoxides and CO_2. The cyclic carbonate-based electrolyte additives were synthesized via the insertion reaction of CO_2 in the corresponding epoxides in a facile two-step procedure. The synthesized electrolyte additives have oxygen as the Lewis base, with a high affinity toward the Lewis-acidic PF_5, which could mitigate HF formation by the stabilization of PF_5 (Scheme 1). Furthermore, the additives contain the acid-responsive acetal group, thereby scavenging HF. First, three epoxides carrying the acetal group were prepared by the reaction of glycidol and vinyl ether-type reactants, producing EEGE, TFGE, and TPGE. The epoxide-bearing trimethoxysilyl group, (3-glycidyloxypropyl) trimethoxysilane (GPTMS), was also prepared in parallel, which is expected to scavenge HF with a different mechanism via the formation of a strong Si−F bond.

Second, the cyclic carbonates were produced by the insertion reaction of CO_2 as a C1 source into epoxides using the organic catalyst 2-(bis(5-(*tert*-butyl)-2-hydroxybenzyl)-amino)-*N*,*N*,*N*-trimethylethan-1-aminium iodide.[30] As it is a bifunctional one-component catalyst for the synthesis of cyclic carbonates bearing both a hydrogen-bonding site and ammonium salts, no cocatalyst such as *n*-Bu_4NI was needed for this coupling reaction. It was also found that only cyclic carbonates were obtained without polymeric species in this insertion reaction. The chemical structures of the prepared

Scheme 1. (a) Schematic Representation of Sequential Hydrolysis Reactions of $LiPF_6$ in the Electrolyte and (b) Synthetic Approach for Various Cyclic Carbonate-Based Electrolyte Additives via the CO_2 Insertion of the Corresponding Epoxide Derivatives

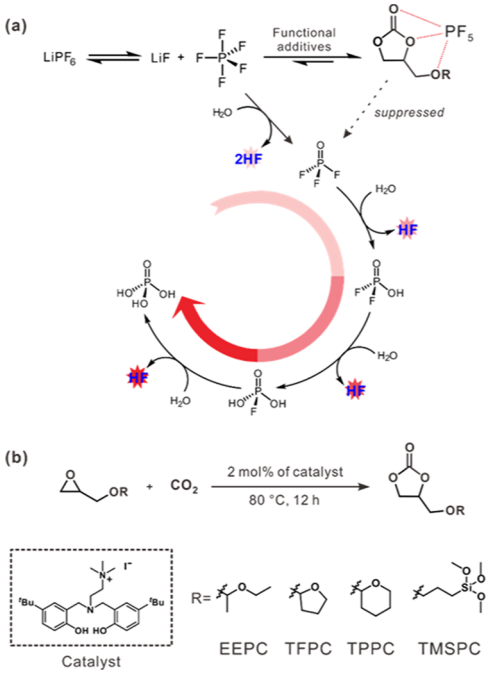

cyclic carbonate additives were successfully confirmed using various NMR spectroscopic techniques, including ^{1}H, ^{13}C, ^{1}H−^{1}H correlation spectroscopy (COSY), and ^{1}H−^{13}C heteronuclear single-quantum correlation (HSQC), as well as high-resolution mass spectrometry (HRMS) (Figures 1 and S1−S5 in the Supporting Information).

The structural properties of the carbonates were clearly characterized by ^{1}H NMR (Figure 1). For example, the disappearance of the epoxide peaks of EEGE (*a*′ and *b*′; 2.50−3.20 ppm) and the appearance of the carbonate peaks of EEPC (*a* and *b*; 4.35−4.90 ppm) indicated the successful coupling

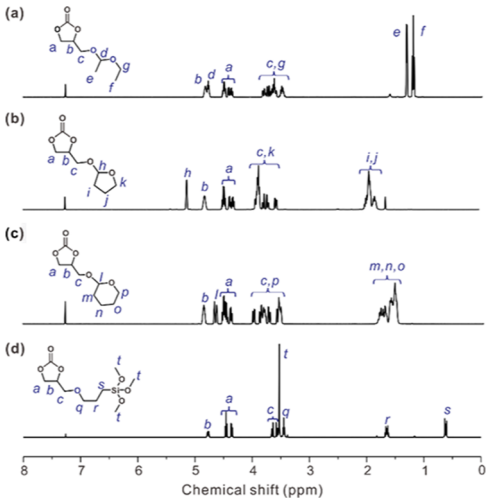

Figure 1. ^{1}H NMR spectra of cyclic carbonate-based additives measured in $CDCl_3$. (a) EEPC, (b) TFPC, (c) TPPC, and (d) TMSPC.

https://dx.doi.org/10.1021/acsami.0c04372
ACS Appl. Mater. Interfaces 2020, 12, 24479−24487

reaction of CO_2. The other complicated peaks could be assigned by tracking the correlation of coupled hydrogens using COSY (Figure S2); a methine proton (*d*; 4.75−4.85 ppm), methylene protons (*c* and *g*; 3.43−3.86 ppm), and methyl protons (*e* and *f*); spectra are attributed to the interaction of neighbored C−H bond; thus, all carbon peaks could be specified along the previously assigned proton. The exact mass agreement of the HRMS spectra also supported the successful synthesis of the well-defined cyclic carbonate derivatives from the corresponding epoxides (Figure S5).

Effect of Cyclic Carbonate-Based Additives on the Stabilization of $LiPF_6$-Containing Electrolytes. We then investigated the energy levels of these synthesized compounds by a computational approach based on DFT calculations. The computational approach compared the highest occupied molecular orbital (HOMO) and lowest unoccupied molecular orbital (LUMO) energy levels of reducible cyclic carbonates such as ethylene carbonate (EC), vinylene carbonate (VC), and fluoroethylene carbonate (FEC) with the cyclic carbonate additives synthesized in this study (Figures 2 and S6). The

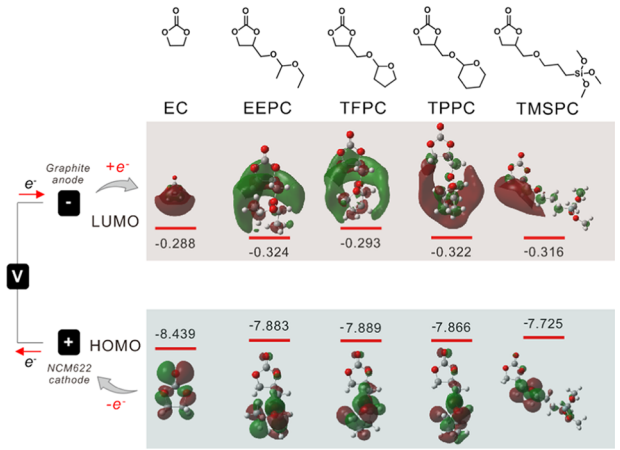

Figure 2. HOMO/LUMO energy levels (eV) of the synthesized cyclic carbonate-based additives with the corresponding chemical structures.

cyclic carbonate derivatives have a relatively high HOMO energy levels (−7.725 to −7.889 eV), implying their high probability of oxidative decomposition prior to the decomposition of EC (−8.439 eV, HOMO) at the cathode. The cyclic carbonate derivatives are mostly consumed in scavenging the PF_5 and HF species generated during the aging process from the hundreds of ppm of physically adsorbed moisture on the graphite anode and NCM622 cathode of a full cell (Figures S7 and S8). Small amounts of the cyclic carbonate derivatives that do not engage in PF_5/HF scavenging may construct the CEI on the cathode and SEI on the graphite anode due to their higher HOMO and lower LUMO energy levels compared to the EC solvent. However, there were no significant differences in the interfacial layers on electrodes precycled in the EEPC- and TMSPC-containing electrolytes (Figure S9).

A fundamental issue that limits the use of $LiPF_6$ is the extremely high reactivity of $LiPF_6$-based electrolytes toward the trace water present in LIBs. Hydrolysis reactions of $LiPF_6$ with water inevitably accompany HF generation. Subsequently, this HF generated produces various phosphoric acid derivatives such as $H(PO_2F_2)$, $H_2(PO_3F)$, and $H_3(PO_4)$, which increase the acidity of the electrolytes (Figure 3a).[9,10]

Moreover, a trace amount of water leads to the generation of reactive POF_3 via irreversible hydrolysis reactions of $LiPF_6$ itself and PF_5 formed by the equilibrium decomposition of $LiPF_6$ (see reactions below)

$$LiPF_6(s) + H_2O(l) \rightarrow LiF(s) + POF_3(g) + 2HF(g) \quad (1)$$

$$PF_5(g) + H_2O(l) \rightarrow POF_3(g) + 2HF(g) \quad (2)$$

The corrosive nature of HF causes the leaching of the SEI components formed on the electrodes. This chemically/physically damaged SEI does not further inhibit the electrolyte decomposition on the reactive electrode surface. The distinctive features of HF are the creation of resistive LiF by the consumption of the limited Li-ion source, and transition-metal dissolution induced from the cathode, indicating the loss of Li-ion storage sites. On first charging (delithiation) of the NCM622 cathode, highly oxidative states of Ni^{4+} are formed in the vicinity of the cathode surface, which is prone to be reduced to the lower oxidation states of Ni^{3+} and Ni^{2+} by accepting electrons from electrolyte components.[33,34] It was reported that the formed Mn^{3+} ions can be converted to Mn^{2+} and Mn^{4+} ions through a disproportionation reaction. Mn^{2+}

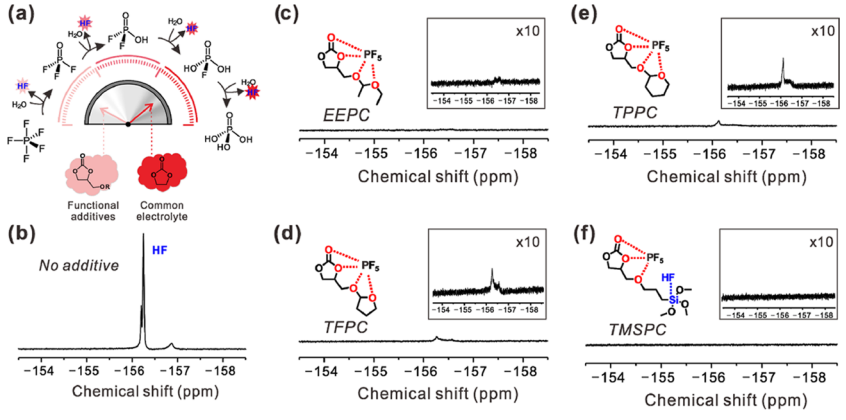

Figure 3. (a) Schematic illustration of the sequential hydrolysis reactions of $LiPF_6$ in the electrolyte (a mixture of EC and EMC in 3:7 v/v). (b−f) ^{19}F NMR spectra of the electrolyte solutions with and without the cyclic carbonate-based electrolyte additives; (b) baseline electrolyte, (c−f) electrolytes in the presence of the additives, (c) EEPC, (d) TFPC, (e) TPPC, and (f) TMSPC after the hydrolysis tests. The samples for ^{19}F NMR analysis were prepared by the addition of 300 ppm of deionized water to the electrolyte.

https://dx.doi.org/10.1021/acsami.0c04372
ACS Appl. Mater. Interfaces 2020, 12, 24479−24487

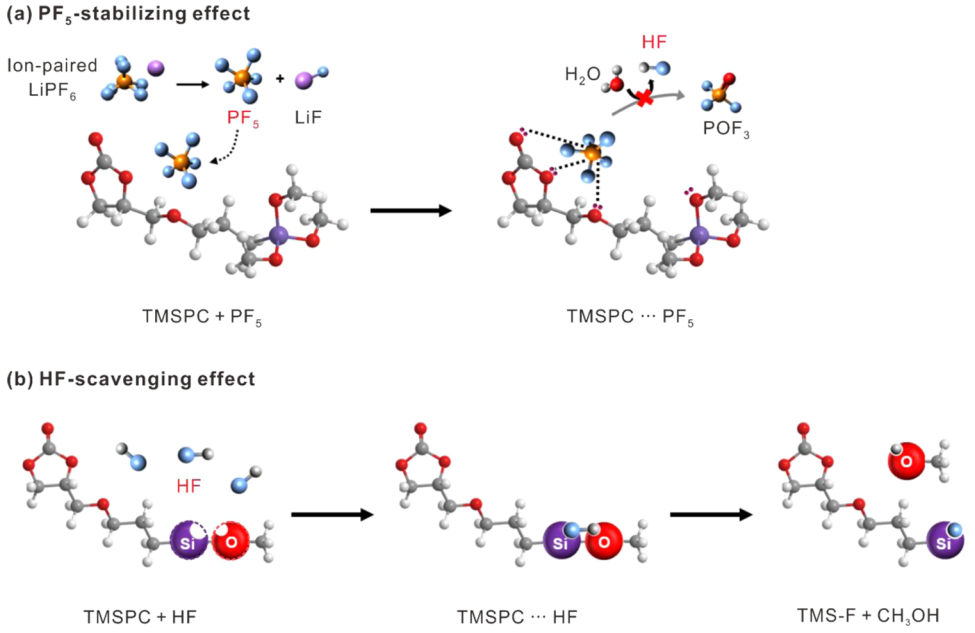

Figure 4. Schematic illustrations of (a) PF_5-stabilizing and (b) HF-scavenging effects by the TMSPC additive.

ions solvated by electrolyte solvent molecules migrate from the cathode to the anode through the electrolyte and deposit on the anode surface, leading to Li extraction from the lithiated anode (Mn^{2+} (aq) + $2LiC_6$ (s) → Mn (s) + $2Li^+$ (aq) + $2C_6$ (s)).[35] Considering the discussion above, it is therefore crucial to employ electrolyte additives that scavenge HF and stabilize PF_5 as a causative agent for HF generation and thereby ensure good battery performances. In this regard, two strategies are generally applicable. The incorporation of a Lewis base with a high affinity toward the Lewis-acidic PF_5, such as phosphorus, oxygen, or nitrogen elements, will mitigate HF generation by PF_5 hydrolysis. A nitrogen core, phosphite, aminosilane, and silyl ether are very effective to scavenge HF and will considerably suppress the increase in the acidity of the electrolyte.[9] In this study, we evaluated the HF-scavenging capability of various cyclic carbonate-based additives by comparing the ^{19}F NMR spectra of the electrolytes in the presence of 3 wt % of water (Figure 3). These newly synthesized cyclic carbonate additives can serve as acid scavengers, specifically, a scavenging Brønsted-acidic HF and Lewis-acidic PF_5. Initially, the characteristic peak intensity of HF at −156.2 ppm was significant in the pristine electrolyte (a mixture of EC and EMC in 3:7 v/v) without additives (Figure 3b). In clear contrast, the characteristic resonance of HF was distinctly reduced in the electrolytes with the cyclic carbonate-based additives. Lone-pair electrons of oxygen from the ether linkages and the cyclic carbonate in the additives (EEPC, TPPC, and TFPC) undergo spatial coordination with the Lewis-acidic PF_5, thereby suppressing HF generation from the hydrolysis of PF_5. Additionally, the ^{31}P NMR results confirmed that these additives inhibit the formation of phosphoric acid derivatives produced by the hydrolysis reactions of $LiPF_6$ (Figure S10). Among the EEPC, TFPC, and TPPC additives containing acetal groups, EEPC showed a relatively higher activity toward the suppression of HF generation (Figure 3c). This result can be explained by the protonation energy barrier (ΔE) of the additives; the energy barrier of the tetrahydropyranyl-substituted acetal of TPPC is the highest, while that of the 1-ethyoxyethyl-substituted acetal of EEPC is the lowest among the three additives carrying acetal groups.[23]

In this case, EEPC can rapidly consume the proton of HF due to its lowest protonation energy barrier. Unlike these acetal-based additives, the TMSPC additive with a silyl ether (Si−O) moiety does not cause HF generation (Figure 3f). This is attributed to both the stabilizing effect of PF_5 with a carbonate-based structure and the preferential interaction with the F^- of HF to form a strong Si−F intermediate (Figure 4). The dual HF-scavenging and PF_5-stabilizing effects of TMSPC help mitigate the increase in the acidity of the electrolyte and will be critical in preserving the well-constructed interface structures of graphite anodes and NCM622 cathodes upon repeated cycling.

Cyclic Carbonate-Based Additives for Long-Term Cycling Stability of NCM622/Graphite Full Cells. The electrochemical performances of an NCM622 cathode coupled with a graphite anode in the potential range between 3.0 and 4.2 V are presented in Figure 5. The cycling stability was evaluated for two representative additives of EEPC and TMSPC, which showed the outstanding capacity for the reduction of the HF content in the electrolyte. Notably, the use of EEPC and TMSPC reduced the overpotential during charging and enhanced the reversible capacity at precycling. The initial Coulombic efficiencies of the full cell with the EEPC-added (87%) and TMSPC-added electrolytes (87%) were higher than that of the pristine electrolyte without the additives (86%). The use of the EEPC and TMSPC additives lead to the elimination of HF, consuming the limited Li^+ ion source that contributes to the reversible capacity of cells; therefore, higher initial Coulombic efficiencies are achieved for the NCM622/graphite full cells with the EEPC- and TMSPC-containing electrolytes.

To explore the impact of the PC-based additive on the rate capability of the NCM622/graphite full cells, cycling was performed at various current densities (Figure 5b). The EEPC- and TMSPC-added electrolytes enhanced the rate performance of the full cells at high current densities compared to the pristine electrolyte without the additives. For instance, the

https://dx.doi.org/10.1021/acsami.0c04372
ACS Appl. Mater. Interfaces 2020, 12, 24479−24487

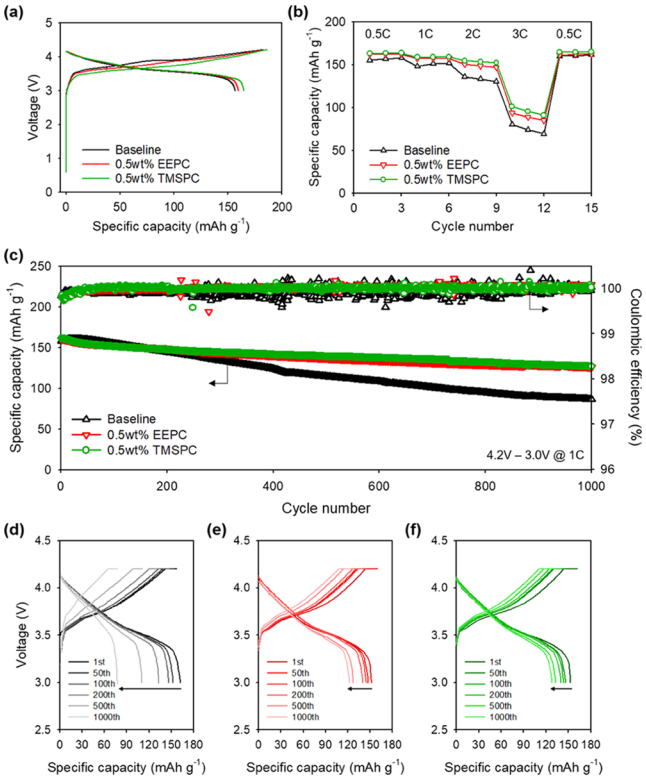

Figure 5. (a) Voltage profiles of NCM622/graphite full cells with the baseline electrolyte, 0.5 wt % EEPC-added electrolyte or 0.5 wt % TMSPC-added electrolyte during precycling at a 0.1C rate and 25 °C. (b) Rate capability of NCM622/graphite full cells at various discharge C rates. (c) Discharge capacity and Coulombic efficiency of NCM622/graphite full cells at a 1C rate and 25 °C during 1000 cycles. (d–f) Voltage profiles of NCM622/graphite full cells with an increasing number of cycles (1, 50, 100, 200, 500, and 1000 cycles) in the (d) baseline electrolyte, (e) 0.5 wt % EEPC-added electrolyte, and (f) 0.5 wt % TMSPC-added electrolyte.

NCM622/graphite full cell with TMSPC delivered a high discharge capacity of 95.7 mAh g^{-1} at a discharge rate of 3C. On the contrary, the electrolyte exhibited rapid capacity fading with increasing current density and delivered a low discharge capacity of 74.0 mAh g^{-1} at a 3C discharge rate. The PF_5-stabilizing ability of the EEPC and TMSPC additives mitigated the HF generation, resulting in the formation of a resistive LiF compound by reaction with the active Li ions at the cathode. It is worth noting that the suppression of LiF formation on the cathode allowed facile charge transport, resulting in a good rate capability of the NCM622/graphite full cells.

A comparison of the cycling performance of the NCM622/graphite full cells at 25 °C demonstrates that the TMSPC- and EEPC-containing electrolytes lead to excellent long-term cycling stability (Figure 5c). The full cells with the EEPC- and TMSPC-added electrolytes displayed an improved discharge capacity retention of 79% and maintained a very high Coulombic efficiency of 100% over 1000 cycles, while the base electrolyte itself showed a relatively steep decrease in the discharge capacity of the full cell. The sluggish capacity decay of cells with the baseline electrolyte, compared to the EEPC- and TMSPC-added electrolytes, is presumed to be due to the thinning of the initially formed SEI/CEI and the exposure of a new surface of electrodes by HF, making the transport of Li^+ ions to the electrode more facile. However, the rapid capacity decay of the cell with the baseline electrolyte is associated with the continued degradation of the electrode–electrolyte interfaces after 100 cycles. Other electrolyte additives such as TFPC and TPPC did not improve the cycling stability of the NCM622/graphite full cells due to their lower activity toward the inhibition of HF generation (Figure S11). Their inferior cycling performance is associated with the poor structural durability of the SEI on the graphite anode and CEI on the NCM622 cathode, induced by the attack of PF_5 and HF that were not eliminated from the electrolyte. It is surmised that the EEPC and TMSPC additives possessing both PF_5-stabilizing and HF-scavenging capabilities minimize the structural degradation of the SEI and CEI layers, leading to the better reversibility of the electrochemical reaction during long-term cycling. Furthermore, the AC impedance spectra clearly show that the EEPC- and TMSPC-containing electrolyte forms a very low-resistance SEI compared to the baseline electrolyte even after 200 cycles (Figure S12) due to the suppression of side reactions by HF and PF_5. This result can be the basis for improving the long-term stability of cycling and is in good agreement with the observation that the EEPC- and TMSPC-containing cells display excellent long-term cycling stability compared to the additive-free electrolyte.

Further evidence of the positive impact of the EEPC and TMSPC additives on the CEI stabilization is presented in Figure S13. The leakage current by the unfavorable electrolyte decomposition at the cathode was also reduced by the incorporation of the EEPC and TMSPC additives. Thus, it is clear that EEPC and TMSPC additives help protect the cathode surface against the oxidative decomposition of electrolyte solvents and salts.

To obtain further insight into the differences between the surface chemistries of the NCM622 cathode with and without the cyclic carbonate-based additives, time-of-flight secondary ion mass spectrometry (TOF-SIMS) and X-ray photoelectron spectroscopy (XPS) were performed after precycling the NCM622/graphite full cells (Figure 6). Strong intensity associated with LiF was observed for the NCM622 cathode surface precycled in the pristine electrolyte (Figure 6a). The resistive LiF on the cathode with the pristine electrolyte led to sluggish Li-ion transport and adversely affected the kinetics of the cathode, resulting in poor long-term cycling stability and rate performance. In contrast, there was a marked change in the LiF_2^- ion map of the cathode surface with the EEPC- and TMSPC-added electrolytes (Figure 6b,c). This is because the EEPC and TMSPC additives can reduce the HF content in the electrolyte, thereby mitigating the formation of LiF on the NCM622 cathode surface. It appears that TMSPC prevents the formation of metal fluorides LiF and NiF_2 on the NCM cathode surface more effectively owing to its silyl ether group, which inhibits the reaction of HF with Li ions (Figure 6b,c). Moreover, the F 1s XPS spectra indicate that the peak intensities attributed to the metal fluorides LiF (684.8 eV) and NiF_2 (685.1 eV) are considerably reduced for the NCM622 cathodes cycled in the EEPC- and TMSPC-containing electrolytes compared to those in the pristine electrolyte. Hence, the suppression of the formation of the resistive CEI components by EEPC and TMSPC improves the overall kinetics of the NCM622 cathodes.

Figure 7 presents the top-view and cross-sectional scanning electron microscopy (SEM) images of the pristine and cycled NCM622 cathodes in the presence of the electrolyte additives. After 1000 cycles, the NCM622 cathodes with EEPC and TMSPC additives appear clean and smooth and, thus, are

https://dx.doi.org/10.1021/acsami.0c04372
ACS Appl. Mater. Interfaces 2020, 12, 24479–24487

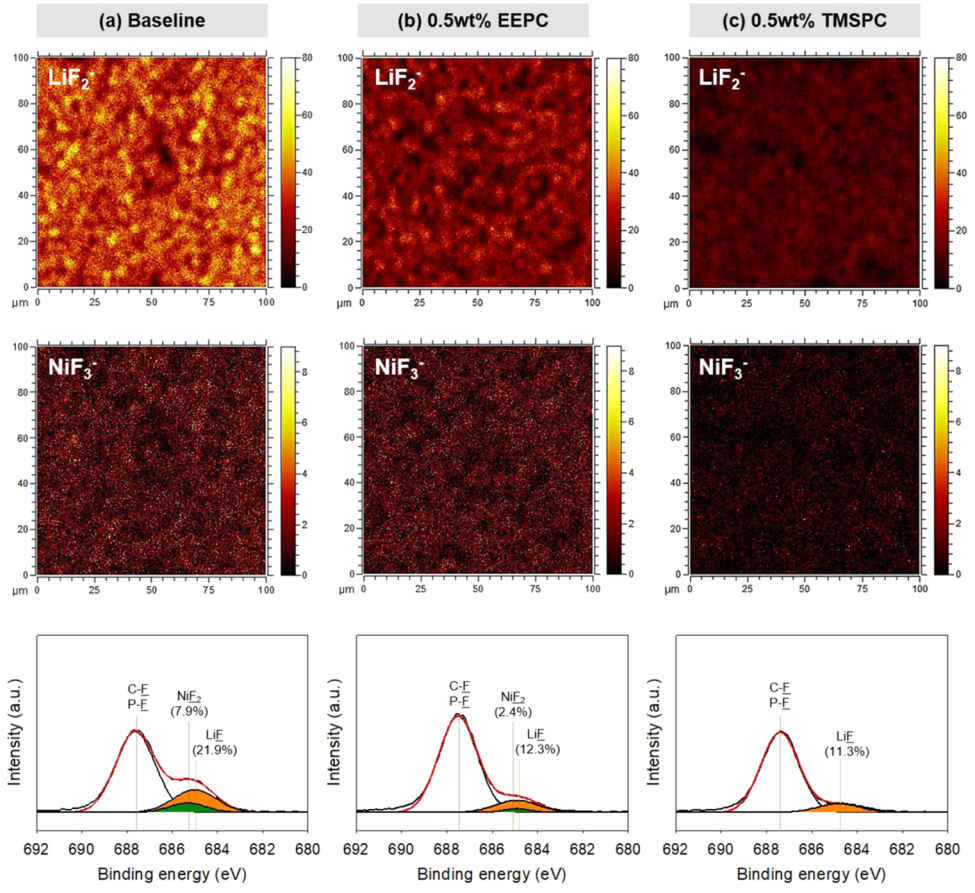

Figure 6. TOF-SIMS images of LiF_2^- (top), NiF_3^- (middle), and the corresponding F 1s XPS spectra (bottom) of the NCM622 cathodes in the (a) baseline electrolyte, (b) electrolyte with the EEPC additive, and (c) electrolyte with the TMSPC additive.

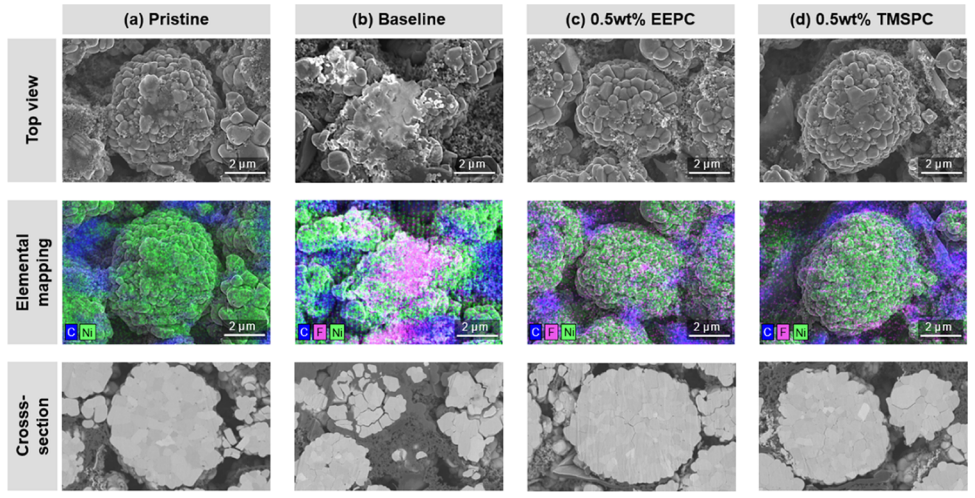

Figure 7. SEM images of electrodes (top panel) top view, (middle panel) elemental mapping images (C, F, and Ni), and (bottom panel) cross-sectional images of (a) pristine NCM622 cathode, (b) NCM622 cathode after 1000 cycles in the baseline electrolyte, (c) NCM622 cathode after 1000 cycles in the EEPC-added electrolyte, and (d) NCM622 cathode after 1000 cycles in the TMSPC-added electrolyte.

comparable to the pristine cathode. However, the NCM622 cathode with the additive-free electrolyte does not maintain the original morphology and is covered by a nonuniform and thick layer. This extremely bumpy surface possibly originates from the CEI attached by HF, which led to the growth of the CEI. Energy-dispersive X-ray spectroscopy (EDS) images revealed that this thick surface layer is composed of species with F, which are highly localized on the cathode particle surface.

Hence, the EEPC and TMSPC additives help preserve the morphological integrity of the cathode through the elimination of HF and PF_5. On the contrary, the additive-free electrolyte caused severe intergranular cracking of the NCM622 cathode composed of aggregated particles. This is mostly due to the HF/PF_5-induced interfacial deterioration of the cathode

https://dx.doi.org/10.1021/acsami.0c04372
ACS Appl. Mater. Interfaces 2020, 12, 24479−24487

particles, resulting in inhomogeneous electrochemical reactions of the cathode. Weakening of the interfacial structure of the cathode caused the infiltration of the electrolyte inside the NCM particles and the accumulation of electrolyte decomposition byproducts, thereby hampering charge transport. Moreover, the additive-free electrolyte formed a nonuniform SEI on the graphite anode compared to the electrolyte with the EEPC and TMSPC additives (Figure S14). The dissolution of transition-metal ions from the severely damaged cathode surface in the additive-free electrolyte is unavoidable; the dissolved transitional metal gets deposited on the graphite anode surface and consumes electrons. This deposited transition metal may act as a catalytic trigger for additional electrolyte decomposition upon prolonged cycling. The nonuniformly reconstructed thick SEI on a specific zone of the graphite surface hinders lithium-ion transfer into the graphite anode structure and accordingly leads to the continued capacity fading of the NCM622/graphite full cells.

CONCLUSIONS

We designed a new class of cyclic carbonate-based electrolyte additives, which deactivate reactive species such as HF and PF_5 produced by the degradation of $LiPF_6$-based electrolytes. The cyclic carbonates were synthesized by an ecofriendly method involving the insertion of CO_2 in functional epoxides. This enabled the use of CO_2 for functional electrolyte additives in LIBs. We evaluated the capability of the synthesized additives to inhibit the generation of phosphoric acid formed by the hydrolysis of $LiPF_6$ using the ^{19}F NMR and ^{31}P NMR spectra of the electrolytes in the presence of functional cyclic carbonate-based additives. The EEPC and TMSPC additives suppressed the activity of HF; the latter showed the best HF scavenging ability along with PF_5 stabilization. The cycling stability, rate capability of NCM622/graphite full cells at various current densities, and long-term cycling stability of the two representative additives, EEPC and TMSPC, were evaluated. The results indicated that the EEPC and TMSPC additives could minimize the structural degradation of the SEI and CEI layers. Furthermore, surface studies of the NCM622 cathode using TOF-SIMS, XPS, and SEM confirmed that the EEPC and TMSPC additives mitigate the interfacial damage to the electrodes caused by highly reactive acidic species such as POF_3, PF_5, and HF. In conclusion, a new class of cyclic carbonate-based electrolyte additives stabilized the Lewis-acidic PF_5, mitigated the formation of Brønsted-acidic HF, and eventually enhanced the rate capability of NCM622/graphite full cells. We anticipate that this study offers a new avenue toward advanced applications of high-energy-density LIBs.

ASSOCIATED CONTENT

Supporting Information

The Supporting Information is available free of charge at https://pubs.acs.org/doi/10.1021/acsami.0c04372.

^1H, ^{13}C, and ^{31}P NMR spectra; $^1H-^1H$ COSY NMR spectra; HSQC NMR spectra of carbonate-based additives; HRMS spectra of carbonate-based additives; XPS spectra of cycled NCM622 cathodes and graphite anodes; electrochemical performance of NCM622/graphite full cells with the synthesized cyclic carbonate-based additives; AC impedance spectra of NCM622/graphite full cells; potentiostatic profiles of NCM622/Li half-cells; and SEM images of cycled anodes (PDF)

AUTHOR INFORMATION

Corresponding Authors

Youngjo Kim − *Department of Chemistry and BK21+ Program Research Team, Chungbuk National University, Cheongju, Chungbuk 28644, Republic of Korea;* orcid.org/0000-0001-8571-0623; Email: ykim@chungbuk.ac.kr

Nam-Soon Choi − *Department of Energy Engineering, School of Energy and Chemical Engineering, Ulsan National Institute of Science and Technology (UNIST), Ulsan 44919, Republic of Korea;* orcid.org/0000-0003-1183-5735; Email: nschoi@unist.ac.kr

Byeong-Su Kim − *Department of Chemistry, Yonsei University, Seoul 03722, Republic of Korea;* orcid.org/0000-0002-6419-3054; Email: bskim19@yonsei.ac.kr

Authors

Jung-Gu Han − *Department of Energy Engineering, School of Energy and Chemical Engineering, Ulsan National Institute of Science and Technology (UNIST), Ulsan 44919, Republic of Korea*

Eunbyul Hwang − *Department of Chemistry, Ulsan National Institute of Science and Technology (UNIST), Ulsan 44919, Republic of Korea; Department of Chemistry, Yonsei University, Seoul 03722, Republic of Korea; Research Center for Green Fine Chemicals, Korea Research Institute of Chemical Technology, Ulsan 44412, Republic of Korea;* orcid.org/0000-0001-5130-7940

Yoseph Kim − *Department of Chemistry and BK21+ Program Research Team, Chungbuk National University, Cheongju, Chungbuk 28644, Republic of Korea*

Sewon Park − *Department of Energy Engineering, School of Energy and Chemical Engineering, Ulsan National Institute of Science and Technology (UNIST), Ulsan 44919, Republic of Korea*

Koeun Kim − *Department of Energy Engineering, School of Energy and Chemical Engineering, Ulsan National Institute of Science and Technology (UNIST), Ulsan 44919, Republic of Korea*

Deok-Ho Roh − *Department of Chemistry, Ulsan National Institute of Science and Technology (UNIST), Ulsan 44919, Republic of Korea*

Minsu Gu − *Department of Chemistry, Yonsei University, Seoul 03722, Republic of Korea;* orcid.org/0000-0002-6270-7496

Sang-Ho Lee − *Research Center for Green Fine Chemicals, Korea Research Institute of Chemical Technology, Ulsan 44412, Republic of Korea;* orcid.org/0000-0003-2207-3369

Tae-Hyuk Kwon − *Department of Chemistry, Ulsan National Institute of Science and Technology (UNIST), Ulsan 44919, Republic of Korea;* orcid.org/0000-0002-1633-6065

Complete contact information is available at: https://pubs.acs.org/10.1021/acsami.0c04372

Author Contributions

#J.-G.H., E.H., and Y.K. contributed equally to this work.

Author Contributions

The manuscript was written through the contribution of all authors. All authors have given approval to the final version of the manuscript.

https://dx.doi.org/10.1021/acsami.0c04372
ACS Appl. Mater. Interfaces 2020, 12, 24479−24487

Notes

The authors declare no competing financial interest.

■ ACKNOWLEDGMENTS

This work was supported by the National Research Foundation of Korea (NRF-2017R1A2B3012148, NRF-2017M3A7B4052802, and NRF-2018R1A2B6004037) and also by the Technology Development Program to Solve Climate Changes of the National Research Foundation (NRF) funded by the Ministry of Science, ICT & Future Planning (2018M1A2A2063341).

■ REFERENCES

(1) Larcher, D.; Tarascon, J. M. Towards Greener and More Sustainable Batteries for Electrical Energy Storage. *Nat. Chem.* **2015**, *7*, 19−29.

(2) Yuan, X.; Liu, X.; Zuo, J. The Development of New Energy Vehicles for a Sustainable Future: A Review. *Renewable Sustainable Energy Rev.* **2015**, *42*, 298−305.

(3) Choi, J. W.; Aurbach, D. Promise and Reality of Post-Lithium-Ion Batteries with High Energy Densities. *Nat. Rev. Mater.* **2016**, *1*, No. 16013.

(4) Hannan, M. A.; Lipu, M. H.; Hussain, A.; Mohamed, A. A Review of Lithium-Ion Battery State of Charge Estimation and Management System in Electric Vehicle Applications: Challenges and Recommendations. *Renewable Sustainable Energy Rev.* **2017**, *78*, 834−854.

(5) Yoo, H. D.; Markevich, E.; Salitra, G.; Sharon, D.; Aurbach, D. On the Challenge of Developing Advanced Technologies for Electrochemical Energy Storage and Conversion. *Mater. Today* **2014**, *17*, 110−121.

(6) Peters, J. F.; Baumann, M.; Zimmermann, B.; Braun, J.; Weil, M. The Environmental Impact of Li-Ion Batteries and the Role of Key Parameters−A Review. *Renewable Sustainable Energy Rev.* **2017**, *67*, 491−506.

(7) Hannan, M.; Hoque, M.; Mohamed, A.; Ayob, A. Review of Energy Storage Systems for Electric Vehicle Applications: Issues and Challenges. *Renewable Sustainable Energy Rev.* **2017**, *69*, 771−789.

(8) Sbordone, D. A.; Di Pietra, B.; Bocci, E. Energy Analysis of a Real Grid Connected Lithium Battery Energy Storage System. *Energy Procedia* **2015**, *75*, 1881−1887.

(9) Han, J.-G.; Kim, K.; Lee, Y.; Choi, N.-S. Scavenging Materials to Stabilize $LiPF_6$-Containing Carbonate-Based Electrolytes for Li-Ion Batteries. *Adv. Mater.* **2019**, *31*, No. 1804822.

(10) Plakhotnyk, A. V.; Ernst, L.; Schmutzler, R. Hydrolysis in the System $LiPF_6$−Propylene Carbonate−Dimethyl Carbonate−H_2O. *J. Fluorine Chem.* **2005**, *126*, 27−31.

(11) Campion, C. L.; Li, W.; Lucht, B. L. Thermal Decomposition of $LiPF_6$-Based Electrolytes for Lithium-Ion Batteries. *J. Electrochem. Soc.* **2005**, *152*, A2327−A2334.

(12) Zhang, X.; Ross, P.; Kostecki, R.; Kong, F.; Sloop, S.; Kerr, J.; Striebel, K.; Cairns, E.; McLarnon, F. Thermal Reactions of Mesocarbon Microbead (MCMB) Particles in $LiPF_6$-Based Electrolyte. *J. Electrochem. Soc.* **2001**, *148*, A463−A470.

(13) Xiao, A.; Li, W.; Lucht, B. L. Thermal Reactions of Mesocarbon Microbead (MCMB) Particles in $LiPF_6$-Based Electrolyte. *J. Power Sources* **2006**, *162*, 1282−1288.

(14) Gnanaraj, J.; Zinigrad, E.; Asraf, L.; Gottlieb, H.; Sprecher, M.; Schmidt, M.; Geissler, W.; Aurbach, D. A Detailed Investigation of the Thermal Reactions of $LiPF_6$ Solution in Organic Carbonates Using ARC and DSC. *J. Electrochem. Soc.* **2003**, *150*, A1533−A1537.

(15) Jang, S. H.; Yim, T. Effect of Silyl Ether-Functinoalized Dimethoxydimethylsilane on Electrochemical Performance of a Ni-Rich NCM Cathode. *ChemPhysChem* **2017**, *18*, 3402−3406.

(16) Li, Y.; Zhang, R.; Liu, J.; Yang, C. Effect of Heptamethyldisilazane as an Additive on the Stability Performance of $LiMn_2O_4$ Cathode for Lithium-Ion Battery. *J. Power Sources* **2009**, *189*, 685−688.

(17) Yamane, H.; Inoue, T.; Fujita, M.; Sano, M. A Causal Study of the Capacity Fading of $Li_{1.01}Mn_{1.99}O_4$ Cathode at 80 °C, and the Suppressing Substances of Its Fading. *J. Power Sources* **2001**, *99*, 60−65.

(18) Wu, X.; Wang, Z.; Li, X.; Guo, H.; Zhang, Y.; Xiao, W. Effect of Lithium Difluoro(oxalato)borate and Heptamethyldisilazane with Different Concentrations on Cycling Performance of $LiMn_2O_4$. *J. Power Sources* **2012**, *204*, 133−138.

(19) Koo, B.; Lee, J.; Lee, Y.; Kim, J. K.; Choi, N.-S. Vinylene Carbonate and Tris(trimethylsilyl) Phosphite Hybrid Additives to Improve the Electrochemical Performance of Spinel Lithium Manganese Oxide/Graphite Cells at 60 °C. *Electrochim. Acta* **2015**, *173*, 750−756.

(20) Song, Y.-M.; Han, J.-G.; Park, S.; Lee, K. T.; Choi, N.-S. A Multifunctional Phosphite-Containing Electrolyte for 5 V-class $LiNi_{0.5}Mn_{1.5}O_4$ Cathodes with Superior Electrochemical Performance. *J. Mater. Chem. A* **2014**, *2*, 9506−9513.

(21) Song, Y.-M.; Kim, C.-K.; Kim, K.-E.; Hong, S. Y.; Choi, N.-S. Exploiting Chemically and Electrochemically Reactive Phosphite Derivatives for High-Voltage Spinel $LiNi_{0.5}Mn_{1.5}O_4$ Cathodes. *J. Power Sources* **2016**, *302*, 22−30.

(22) Han, J.-G.; Lee, S. J.; Lee, J.; Kim, J. S.; Lee, K. T.; Choi, N.-S. Tunable and Robust Phosphite-Derived Surface Film to Protect Lithium-Rich Cathodes in Lithium-Ion Batteries. *ACS Appl. Mater. Interfaces* **2015**, *7*, 8319−8329.

(23) Hwang, E.; Kim, K.; Lee, C. G.; Kwon, T.-H.; Lee, S.-H.; Min, S. K.; Kim, B.-S. Tailorable Degradation of pH-Responsive All-Polyether Micelles: Unveiling the Role of Monomer Structure and Hydrophilic−Hydrophobic Balance. *Macromolecules* **2019**, *52*, 5884−5893.

(24) Fitton, A. O.; Hill, J.; Jane, D. E.; Millar, R. Synthesis of Simple Oxetanes Carrying Reactive 2-Substituents. *Synthesis* **1987**, *1987*, 1140−1142.

(25) Song, J.; Palanikumar, L.; Choi, Y.; Kim, I.; Heo, T.-y.; Ahn, E.; Choi, S.-H.; Lee, E.; Shibasaki, Y.; Ryu, J.-H.; et al. The Power of the Ring: a pH-Responsive Hydrophobic Epoxide Monomer for Superior Micelle Stability. *Polym. Chem.* **2017**, *8*, 7119−7132.

(26) Shriver, D. F.; Drezdzon, M. A.; Drezdzon, M. A. *The Manipulation of Air-Sensitive Compounds*; John Wiley & Sons, 1986.

(27) Girolami, G. S.; Rauchfuss, T. B.; Angelici, R. J. *Synthesis and Technique in Inorganic Chemistry: A Laboratory Manual*; University Science Books, 1999.

(28) Armarego, W. L. *Purification of Laboratory Chemicals*; Butterworth-Heinemann, 2017.

(29) Pangborn, A. B.; Giardello, M. A.; Grubbs, R. H.; Rosen, R. K.; Timmers, F. J. Safe and Convenient Procedure for Solvent Purification. *Organometallics* **1996**, *15*, 1518−1520.

(30) Hong, M.; Kim, Y.; Kim, H.; Cho, H. J.; Baik, M. H.; Kim, Y. Scorpionate Catalysts for Coupling CO_2 and Epoxides to Cyclic Carbonates: A Rational Design Approach for Organocatalysts. *J. Org. Chem.* **2018**, *83*, 9370−9380.

(31) Hohenberg, P.; Kohn, W. Inhomogeneous Electron Gas. *Phys. Rev.* **1964**, *136*, B864−B871.

(32) Frisch, M.; Trucks, G.; Schlegel, H.; Scuseria, G.; Robb, M.; Cheeseman, J.; Scalmani, G.; Barone, V.; Mennucci, B.; Petersson, G. *Gaussian 09*, revision A.02; Gaussian, Inc.: Wallingford, CT, 2016.

(33) Zhan, C.; Wu, T.; Lu, J.; Amine, K. Dissolution, Migration, and Deposition of Transition Metal Ions in Li-Ion Batteries Exemplified by Mn-Based Cathodes−A Critical Review. *Energy Environ. Sci.* **2018**, *11*, 243−257.

(34) Gilbert, J. A.; Shkrob, I. A.; Abraham, D. P. Transition Metal Dissolution, Ion Migration, Electrocatalytic Reduction and Capacity Loss in Lithium-Ion Full Cells. *J. Electrochem. Soc.* **2017**, *164*, A389−A399.

(35) Choi, N.-S.; Yeon, J.-T.; Lee, Y.-W.; Han, J.-G.; Lee, K. T.; Kim, S.-S. Degradation of Spinel Lithium Manganese Oxides by Low Oxidation Durability of $LiPF_6$-Based Electrolyte at 60 °C. *Solid State Ionics* **2012**, *219*, 41−48.

https://dx.doi.org/10.1021/acsami.0c04372
ACS Appl. Mater. Interfaces 2020, 12, 24479−24487